Aust. J. Phys., 1995, **48**, 543–56

The Dielectric Barrier Discharge: A Bright Spark for Australia's Future*

D. S. Newman[A] *and M. J. Brennan*[B]

[A] Department of Applied Physics, Central Queensland University, Rockhampton, Qld 4702, Australia.

[B] Electron Physics Group, Research School of Physical Sciences & Engineering, Australian National University, Canberra, ACT 0200, Australia.

Abstract

A dielectric barrier or silent discharge is the name given to a transient gas discharge occurring between two electrodes separated by one or two layers of dielectric material. They have formed the basis of commercial ozonisers for nearly a century but, despite the maturity of this technology, significant experimental and theoretical questions remain to be answered about the operation of these discharges before they can be fully exploited in new applications. Of particular interest is the potential that dielectric barrier discharges display for development as sources of intense, monochromatic, incoherent UV/VUV radiation. This paper briefly outlines the current status of the field with regard to research into the operation and UV/VUV radiative spectroscopy of dielectric barrier discharges. Some applications of these sources are briefly discussed and some of the theoretical models proposed to explain their operation are outlined. The paper concludes with a summary and outlook of the experimental and theoretical project that is being set up under a collaborative venture by CQU and ANU to study dielectric barrier discharges.

1. Introduction

The silent or dielectric barrier discharge was first described by Siemens (1857) and proposed as a direct method of dissociating oxygen to produce ozone from air. Such a discharge typically consists of two electrodes in a coaxial or planar arrangement, separated by a gap containing one or two layers of dielectric material as shown in Fig. 1. It generally operates at gas pressures ranging from 100 mbar to a few atmospheres and electric fields of 0·1–10 kV cm^{-1}. It is an AC device, capable of working over a wide range of driving frequencies ranging from single pulse to 100 kHz or more. The discharge normally consists of a multitude of individual microdischarges randomly distributed throughout the discharge volume. The insulating properties of the dielectric barrier ensure an even spatial distribution of microdischarges and also limit their charge buildup and duration, effectively shutting them off after a few nanoseconds. Each microdischarge takes the form of a luminous current filament of roughly cylindrical cross section with a diameter of approximately 100 μm. The electron density in a microdischarge is typically of the order of 10^{14}–10^{15} cm^{-3}, corresponding to a weakly ionised plasma state with mean electron energies ranging from 0·1–20 eV (Gellert and

* Refereed paper based on a contribution to the Third Japan-Australia Workshop on Gaseous Electronics and Its Applications, held in Yeppoon, Queensland, in July 1994.

0004-9506/95/030543$05.00

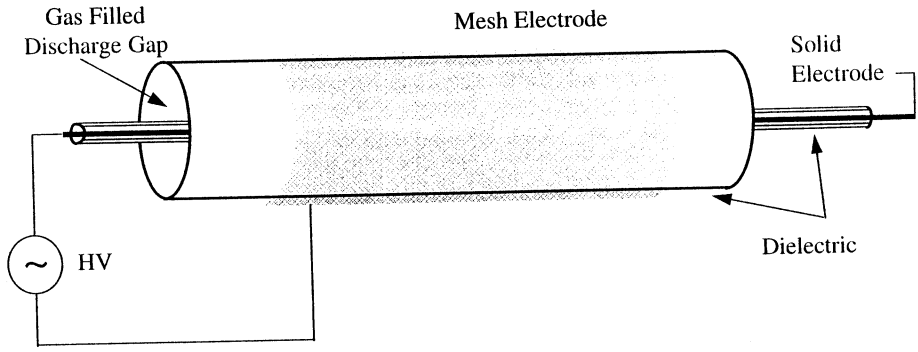

Fig. 1. Schematic diagram of a co-axial dielectric barrier discharge configured with a mesh outer electrode, for use as a UV source. In this configuration, both the inner and outer electrodes are covered with dielectric material, transparent to the UV wavelengths produced in the discharge.

Kogelschatz 1991). Thus, the electrons in the microdischarge are not usually in local thermal equilibrium (LTE) with the ionic or neutral species which possess thermal energies only. Away from the dielectric boundaries, however, the electrons can be considered to be in equilibrium with the instantaneous local electric field. As the microdischarge develops, charge builds up on the dielectric boundary and results in a reduction in the local electric field within the current filament. When this has dropped sufficiently so that the maximum possible electron energy falls below the ionisation thresholds of the neutral species present, attachment and recombination processes take over to choke the microdischarge.

In the following sections of this paper, some practical applications utilising the radiative capabilities of dielectric barrier discharges are outlined. The generation of UV/VUV radiation and spectroscopic investigations of the radiation from the sources are briefly reviewed, along with some of the theoretical modeling that has been undertaken to describe the ignition, evolution and kinetic processes occurring in individual microdischarges. The experimental apparatus under construction at CQU to study these phenomena is described and the paper concludes with a discussion of the weaknesses in our present understanding of dielectric barrier discharges and outlines the possible directions of the experimental and theoretical investigations in the CQU–ANU collaborative venture.

2. Practical Applications of Dielectric Barrier Discharges

In many processing applications, the key requirement for a useful plasma is that it generates a large flux of energetic electrons which can then be used to initiate or enhance a variety of chemical, biological and physical processes. The relatively high voltage, high pressure configurations which are the norm for dielectric barrier discharges, provide particularly appropriate conditions for the generation of highly energetic electrons. The dielectric barrier discharge is arguably one of the most commercially significant non-LTE discharges given that the ozoniser, being its earliest industrial application, has proven to be a viable technological development since the turn of the century. Modern ozonisers consist of large parallel arrays of annular discharge sources, each similar to

that shown in Fig. 1, with a length of 1–2 m and a small discharge gap of 0·5–3 mm. They are air fed devices, operating at pressures of 1–3 atmospheres (1 atmosphere = 101·325 kPa). The applied voltages are typically in the range 0·5–20 kV and switched at frequencies of between 50 Hz–5 kHz.

The formation of ozone from discharges in pure oxygen or air results from a very complex set of reactions. There have been many attempts to model the operation of ozonisers to improve their efficiency and yield (Yagi *et al.* 1979; Eliasson and Egli 1987; Eliasson *et al.* 1987; Braun *et al.* 1991). One of the major limitations to their productivity arises from dissociative reactions between ozone and energetic electrons and ions formed in the discharge. To eliminate the impact of these reactions on the production of ozone, Eliasson and Kogelschatz (1991*a*) investigated the use of UV radiation to initiate the primary photodissociation of oxygen. Photons of 172 nm wavelength were produced by the decay of xenon excimers formed in a cylindrical dielectric barrier discharge source and used to irradiate air flowing through a surrounding concentric volume. Their results did not show any marked advantage over the standard barrier discharge ozoniser configuration, but raised many questions concerning the operation of their apparatus and demonstrated that further work still has to be undertaken in this area.

Other applications of UV lamps based on dielectric barrier discharge sources have started to emerge in recent years. The plasma–chemical and photochemical processing potential of these devices has been recognised and various groups are investigating their use in a variety of environmental and industrial situations. Kogelschatz (1993) and Nohr *et al.* (1994) have proposed designs for photoreactors incorporating silent discharge excimer UV lamps as integral elements to undertake photodegradation of pollutants. These photo-induced processes will require high radiation intensities, probably at specific UV/VUV wavelengths, to be of practical or commercial interest.

The semiconductor industry represents a major area in which efficient sources of UV radiation could be employed. Many groups are now investigating the production of thin films by laser chemical vapour deposition using excimer lasers to provide the UV radiation (see for example Mukaida *et al.* 1993 and Xiong *et al.* 1993). The high localised intensities, coherence and pulsed nature of laser radiation are not necessarily required for these processes. A moderately intense source operating over large areas in a continuous manner may prove just as useful, if not more so. Some pilot studies have already been performed to modify surfaces and deposit thin films using excimer generated UV radiation from dielectric barrier discharges (Esrom and Kogelschatz 1992; Bergonzo *et al.* 1993; Bergonzo and Boyd 1993; Manfredotti *et al.* 1993; Zhang *et al.* 1993, 1994). The dielectric barrier discharge sources used in these studies were not optimised and yet still displayed great promise for low temperature processing of materials.

3. Spectroscopic Studies of the Emitted Radiation

Initial studies of UV and VUV radiation emission from dielectric barrier discharges most probably developed from experimental investigations aimed at finding alternative emission sources to hydrogen, helium and Lyman continua. Several authors described the continuous emission spectra of various rare gases at pressures up to about 500 Torr (1 Torr = 133 Pa), excited by microwave

and transformer discharges (Tanaka and Zelikoff 1954*a*, 1954*b*; Tanaka 1955; Huffman *et al.* 1963; Wilkinson and Byram 1965). The emission bands observed were attributed to excimer radiation from the formation and decay of rare gas dimers, based on the work of Hopfield (1930*a*, 1930*b*, 1930*c*) and McLennan and Turnbull (1930, 1933). Other techniques employed for the study of continuous emission spectra in the VUV include the observation of dc discharge afterglows (Wieme and Lenaerts 1981) and measurements on constricted glow discharges at pressures between 100 and 500 mbar (Lindau and Dobele 1988).

Microwave excited discharges have also been extensively investigated as possible sources of high intensity UV radiation. Kumagai and Obara (1989*a*, 1989*b*, 1989*c*) have studied the radiative efficiency of ArF and KrF in a He/Ne buffer, contained in a quartz sphere and excited by a microwave oscillator and magnetron tube operating at a frequency of 2·45 GHz. KrF ($B \rightarrow X$) fluorescence at pulse lengths of 5 μs duration at operational frequencies up to 55 kHz was produced with an intrinsic efficiency of up to 12·5%. Intrinsic efficiency is defined as the ratio of the excimer radiation fluorescence power to the microwave (or other) power deposited in the discharge. Similar measurements for ArF ($B \rightarrow X$) fluorescence achieved pulses of 8 ms duration at a frequency of 100 Hz resulting in an intrinsic efficiency of 4·4%. These experiments were later extended by Nakamura *et al.* (1990) using an Ar buffer in the Kr and F mixture to obtain dual wavelength emission from ArF and KrF in the same lamp. It is also interesting to note here that Gerber *et al.* (1980) reported a KrF excimer flashlamp based on a capillary discharge and achieved an intrinsic efficiency of 28%.

Experiments aimed specifically at the study of excimer radiation emission from dielectric barrier discharges were reported by Shuaibov and Shevera (1979), Shevera and Shuaibov (1980), Pavlovskaya and Yakovleva (1983) and Volkova *et al.* (1984). The bulk of this work was aimed at developing a radiation source suitable for absorption studies in the UV and VUV regions of the spectrum and observations were made of the continuous emission spectra of Xe, Kr and Ar as a function of their concentration in various buffer gases and also their mixtures with halogen carriers (SF_6, CF_2Cl_2 and CH_2Br_2). However, the most comprehensive studies of radiation emission from these sources have been undertaken by Kogelschatz and co-workers at the Asea Brown Boveri Research Laboratories in Baden, Switzerland. The initial impetus for their work came from a desire to investigate whether a UV source could be developed to dissociate oxygen and produce ozone more efficiently than conventional ozonisers. In the remainder of this section, we shall discuss the work of these researchers in some detail as it represents the current status of the field as regards the spectroscopic investigations of these sources.

Eliasson and Kogelschatz (1988) reported experimental and theoretical investigations of the molecular continuum radiation from Xe_2 at 172 nm in a planar discharge source containing one dielectric barrier. This work was extended by Gellert and Kogelschatz (1991) who studied the emission of radiation from a variety of excimers using two experimental configurations, a cylindrical discharge source constructed from Suprasil 1 quartz to observe radiation emitted at wavelengths greater than 150 nm and a glass source with a LiF window for measurements at shorter wavelengths. Spectra were recorded using a 0·3 m VUV spectrograph

Table 1. Radiative features observed in various excimer systems (from Gellert and Kogelschatz 1991)

Excimer	Transition	λ_{max} (nm)	Remarks
Xe_2	$B \rightarrow X$	172	Approx. 14 nm FWHM
Kr_2	$B \rightarrow X$	146	Approx. 13 nm FWHM
Ar_2	$B \rightarrow X$	126	Approx. 10 nm FWHM
F_2	$D' \rightarrow A'$	158	2% F_2 in He, approx. 3 nm FWHM
Cl_2	$D' \rightarrow A'$	259	5% Cl_2 in Ar, approx 5 nm FWHM
Br_2	$D' \rightarrow A'$	289	Approx. 7 nm FWHM, pronounced peak asymmetry
I_2	$D' \rightarrow A'$	342	2% I_2 in Ar, approx. 7 nm FWHM, pronounced peak asymmetry
ArCl*	$B \rightarrow X$	175	Approx. 3 nm FWHM
KrCl*	$B \rightarrow X$	222	Approx. 3 nm FWHM
XeCl*	$B \rightarrow X$	308	Aprox. 5 nm FWHM
	$B \rightarrow A/C \rightarrow A$	330–55	Broad, low intensity feature
ArF*	$B \rightarrow X$	193	Approx. 5 nm FWHM
	$B \rightarrow A$	220	
KrF*	$B \rightarrow X$	249	Approx. 5 nm FWHM
	$D \rightarrow X/C \rightarrow A$	260–90	Very weak, broad feature
XeF*	$B \rightarrow X$	351	Approx. 5 nm FWHM
	$C \rightarrow A$	460	Very weak, broad feature
ArBr*	$B \rightarrow X$	165	Approx. 2 nm FWHM
	$D \rightarrow X$	172	
KrBr*	$B \rightarrow X$	207	Approx. 2 nm FWHM
	$C \rightarrow A$	222	Weak shoulder on $B \rightarrow A$ peak
	$B \rightarrow A$	228	Approx. 10% of $B \rightarrow X$ intensity
XeBr*	$B \rightarrow X$	283	Approx. 2 nm FWHM, UV efficiency estimated at 10%
	$C \rightarrow A/B \rightarrow A$	300–40	Very weak, broad feature
KrI*	$B \rightarrow X$	190	
	$B \rightarrow A$	225	
XeI*	$B \rightarrow X$	253	
	$B \rightarrow A$	320	Approx. 25% of $B \rightarrow X$ intensity

coupled to an optical multichannel analyser. Both sources were chemically cleaned by gas discharge sputtering and evacuated to base pressures of better than 10^{-7} mbar by a turbomolecular pump before filling with high purity gases. The experiments were undertaken with the source operating in the fully established microdischarge mode and investigated excimer radiation generation by pure rare gases, rare gas–halogen mixtures, halogen dimers and mercury–rare gas/halogen mixtures. UV, VUV and visible radiation emission was observed for a large number of excimers with efficiencies varying from 1–10% and bandwidths of 1–17 nm FWHM. A summary of the results of these measurements is presented in Table 1. Some typical examples of the spectra obtained are presented in Fig. 2 which shows three rare gas–chloride excimers. These are dominated by the Rg^+Cl^- $B(^2\Sigma)$ to RgCl $X(^2\Sigma)$ transitions which give rise to the usual lasing transitions. The peaks also demonstrate a slight asymmetry towards the blue which can be attributed to pressure dependent effects. At the pressures employed in the discharge tube, higher vibrational transitions have not been fully quenched and appear as an unresolved high energy wing on each of the spectra. In addition there are also some broad, weak structures present in the KrCl* and XeCl* spectra due to transitions from high lying electronically excited states to the repulsive $A(^2\Pi)$ state.

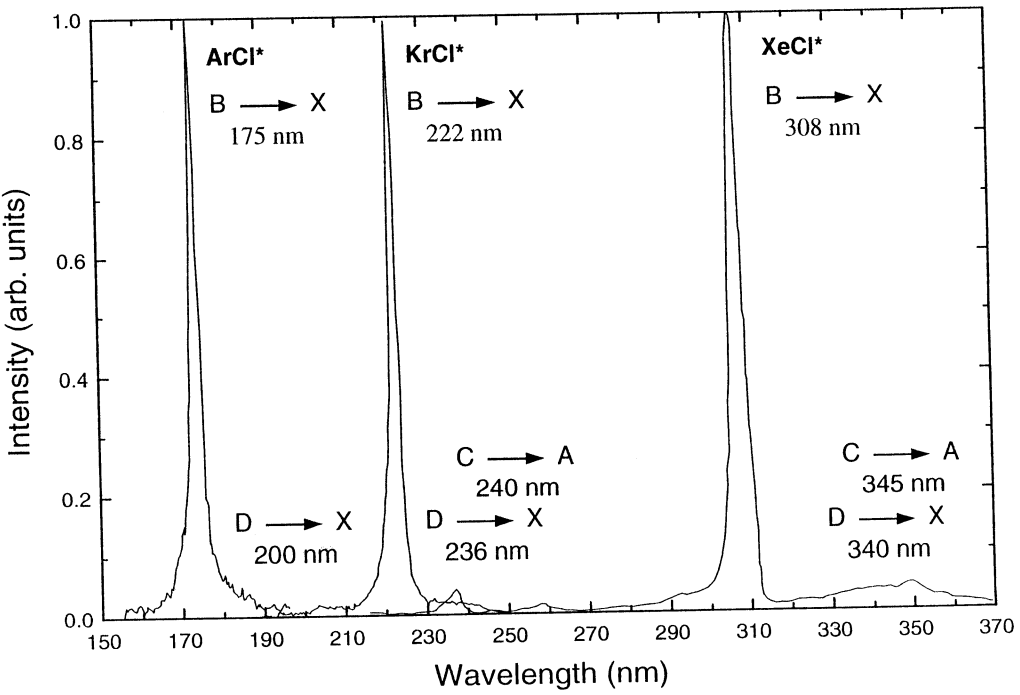

Fig. 2. Emission spectra of rare gas–chloride excimers in a dielectric barrier discharge (from Gellert and Kogelschatz 1991).

Eliasson and Gellert (1990) measured radiation emission from mercury–rare gas mixtures in an apparatus similar to that described above but which could be externally heated to 250°C. By operating the dielectric barrier discharge source in a low pressure mode, a glow discharge was produced and the intensity of mercury resonance radiation was measured at various temperatures and pressures using a low resolution spectrometer. At higher buffer gas pressures, excimer radiation was observed and investigated as a function of source temperature with a high resolution spectrometer. They determined that few excimers were formed in the discharges with Ar, Ne or He, the spectra of which displayed increasing radiation trapping of the Hg resonance lines as the source temperature was increased. The intensity from Hg–Kr mixtures was approximately a factor of five below that for Hg–Xe which displayed the strongest emission. Emission bands A–F of the Hg–Xe dimer were observed, though bands E and F were of very low intensity. Radiation trapping of Hg resonance radiation was not readily apparent in this mixture as the source temperature was increased and was attributed to an increasing concentration of HgXe excimers resulting in fewer free Hg atoms in the discharge volume. Eliasson and Gellert also estimated the Boltzmann temperature of the discharge as a function of source temperature and demonstrated that external heating could be employed to tune the source to maximise radiation emission at a particular wavelength (172, 185 or 254 nm for Hg–Xe mixtures). Table 2 summarises some of the results of the radiative features of the Hg–rare gas excimers from these measurements.

Table 2. Radiative features observed from the HgXe excimer (from Eliasson and Gellert 1990)

State	λ_{max} (nm)	Remarks
A^30^+	260–75	
B^31	253–54	
C^32	235–45	
D^31	≈225	
E^11	210–20	Very weak
F^10^+	184–86	Very weak

Models were developed by the authors to explain the formation of excimers in these sources. They will be described in more detail in the following section but discharge evolution, charged particle kinetics and excimer and excited species generation were included. The complexity of the modelling process can be appreciated from the calculations on the Hg–Xe mixture for example, in which 33 species and 80 reactions were taken into consideration.

4. Theoretical Simulation of Microdischarge Physics

In this section, three numerical simulations of silent discharge operation due to Morrow and Sato (1990), Eliasson and Kogelschatz (1991*b*) and Pietsch *et al.* (1993) will be discussed. Morrow and Sato limited their treatment to a one-dimensional case to compare the electric field distributions between rf discharges with and without insulators in the discharge gap, whereas Eliasson and Kogelschatz and Pietsch *et al.* have attempted to fully model the ignition, evolution and extinction of microdischarges in the silent discharge process. All of the models employed the same geometrical configuration of two planar metallic electrodes, one of which was covered by a layer of dielectric material, with the discharge occurring in the gap between the dielectric and the bare electrode.

The basic approaches to the calculations can be summarised as follows. In principle, it is necessary to solve a set of coupled Boltzmann equations for each species in the discharge but in practice, a number of assumptions can be made to simplify the computations. These include that all heavy particles can be considered at rest compared to the electrons, electron-electron and electron–ion interactions can be neglected and isotropic electron scattering occurs. In addition, Monte Carlo calculations have shown that, under the conditions of the discharge, the electron energy distribution is always in local equilibrium with the electric field (Eliasson and Egli 1987; Pietsch *et al.* 1993). These assumptions serve to reduce the calculation to the solution of a coupled set of continuity equations for each species which take the form of

$$\frac{\partial n_i(\boldsymbol{r}, t)}{\partial t} + \nabla \cdot \{n_i(\boldsymbol{r}, t)\boldsymbol{W}_i(E/n)\} - \nabla \cdot \{D_i(E/n) \cdot \nabla n_i(\boldsymbol{r}, t)\} = S_i(n_1, \ldots, n_m)(E/n)\,,$$

where $n_i(\boldsymbol{r}, t)$ is the concentration of particles i, $\boldsymbol{W}_i(E/n)$ is the drift velocity, E/n is the reduced electric field, $D_i(E/n)$ is the diffusion coefficient and

$S_i(n_1, \ldots, n_m)(E/n)$ is the sum of all source and sink terms for the reactions in which the ith particles figure.

The electron transport coefficients and rate coefficients for electron collision processes are affected by the local values of the electric field throughout the discharge volume and on the dielectric surface. The electric field distribution is obtained by solving Poissons equation for a potential $\Phi(\boldsymbol{r}, t)$, subject to suitable boundary conditions at the electrode and dielectric surfaces,

$$\nabla^2\Phi(\boldsymbol{r}, t) = -\frac{\rho(\boldsymbol{r}, t)}{\epsilon_0},$$

where the space charge distribution is given by

$$\rho(\boldsymbol{r}, t) = n_+(\boldsymbol{r}, t) + n_-(\boldsymbol{r}, t) + n_e(\boldsymbol{r}, t),$$

and n_+, n_- and n_e are the positive and negative ion and electron densities respectively. The electric field $\boldsymbol{E}(\boldsymbol{r}, t)$ can then be calculated from

$$\boldsymbol{E}(\boldsymbol{r}, t) = -\nabla\Phi(\boldsymbol{r}, t).$$

The value of the local electric field is then used to determine the electron energy distribution function using the stationary Boltzmann equation, from which the local charged particle densities for each species $\partial n_i(\boldsymbol{r}, t)/t$ can be derived from the chemical rate equations for their production.

Morrow and Sato (1990) did not attempt to describe the evolution of a microdischarge but were more interested in examining the temporal variation of charge build-up on the dielectric surface. They simplified their simulation by neglecting source terms such as ionisation, attachment, recombination and secondary emission from the electrodes as well as all non-equilibrium effects. Their calculation was initialised with a uniform distribution of nitrogen at a pressure of 0·13 kPa and an electron density of 10^{15} m^{-3} in the source and they considered the application of dc and radio-frequency (10 MHz) voltages to the insulator covered electrode while holding the bare electrode at ground potential. One-dimensional continuity equations for electrons and ions were solved using a flux corrected transport (FCT) algorithm with simultaneous solution of Poissons equation to obtain the local electric field. They determined that a cathode fall region developed in front of both the bare electrode and insulator, in accordance with the polarity of the applied voltage, due to electrons moving away from the cathode leaving a high positive ion density. An unexpected result arose when, despite their greatly different mobilities, positive ions were found to be as effective as electrons for charging the dielectric surface over a time scale comparable to one half cycle of the applied radio-frequency voltage.

Eliasson and Kogelschatz (1988, 1991*b*) modelled the silent discharge as an interplay between the discharge physics and the plasma chemistry occurring in the discharge gap. The discharge physics model treated the formation of electrons, ions and excited species following the application of the electric field and yielded similar results to those of Pietsch *et al.* (1993) discussed below. The plasma chemistry model described the chemical reactions between the various species

and is illustrated here using the results of their calculations for the production of UV/VUV radiation from a discharge in pure xenon at a pressure of 1000 mbar. A simplified model of the xenon system was employed involving electrons, ground state Xe, Xe^+ and Xe_2^+ ions and grouping all of the excited states of atomic and molecular xenon into four levels, Xe*, Xe**, Xe_2* and Xe_2**. The species number densities were calculated using a scheme of 25 reactions. UV radiation of wavelength 172 nm is produced from the decay of the Xe_2* excimer to its ground state which subsequently dissociates into two Xe atoms:

$$Xe_2^* \rightarrow 2Xe + h\nu \quad (\lambda = 172 \text{ nm}).$$

The direct production of Xe_2^* arises from the Xe* state according to

$$Xe^* + 2Xe \rightarrow Xe_2^* + Xe,$$

but other indirect mechanisms involving deactivation of Xe** and Xe_2** and ionic recombination processes from Xe^+ and Xe_2^+ were also considered. The radiative decay process also competes with quenching of Xe_2* by itself (electron density dependent) and by Xe (pressure dependent) according to

$$Xe_2^* + Xe_2^* \rightarrow 2Xe + Xe_2^+ + e, \qquad Xe_2^* + Xe \rightarrow Xe^* + Xe + Xe.$$

The results of the calculation are shown in Figs 3*a* and 3*b* which illustrate the particle densities and UV output respectively at 172 nm as a function of time in the microdischarge. The efficiency of the process for generating UV photons can then be obtained as a function of pressure or E/n by repeated calculation. These computations yielded intrinsic efficiencies of up to 45% at electron densities of 10^7 cm^{-3} and reduced fields of about 40 Td in agreement with the work of Eckstrom *et al.* (1988). From their experimental results, Eliasson and Kogelschatz obtained UV efficiencies of 5–10% which corresponded to an estimated intrinsic efficiency of 15–30% in their apparatus.

Pietsch *et al.* (1993) computed the spatial and temporal evolution of a microdischarge under dc conditions with an FCT algorithm using a two-dimensional grid. Their model identified four phases in the development of a microdischarge; Townsend, streamer, cathode layer formation and decay. In the Townsend phase, there exists a high, undisturbed electric field across the gap which results in electrical breakdown. The electron avalanches generated can be described by Townsend's first ionisation coefficient and last for about 10 ns. In the streamer phase, a high space charge of positive ions exists in front of the anode which results in a cathode directed streamer that lasts for about 3–4 ns. At this time the electron number density increases rapidly and the highest electric field strengths occur in the microdischarge column. About 1 ns after streamer arrival at the cathode, a fall region forms which is about 10 μm wide and supports a potential difference of several hundred volts. A steep rise in current occurs at this stage. Following this comes the decay phase in which the current flow is determined by the physical properties of the discharge source such as dielectric barrier material and thickness and external circuit configuration. Charges that are deposited on the dielectric surface gradually reduce the mean electric field

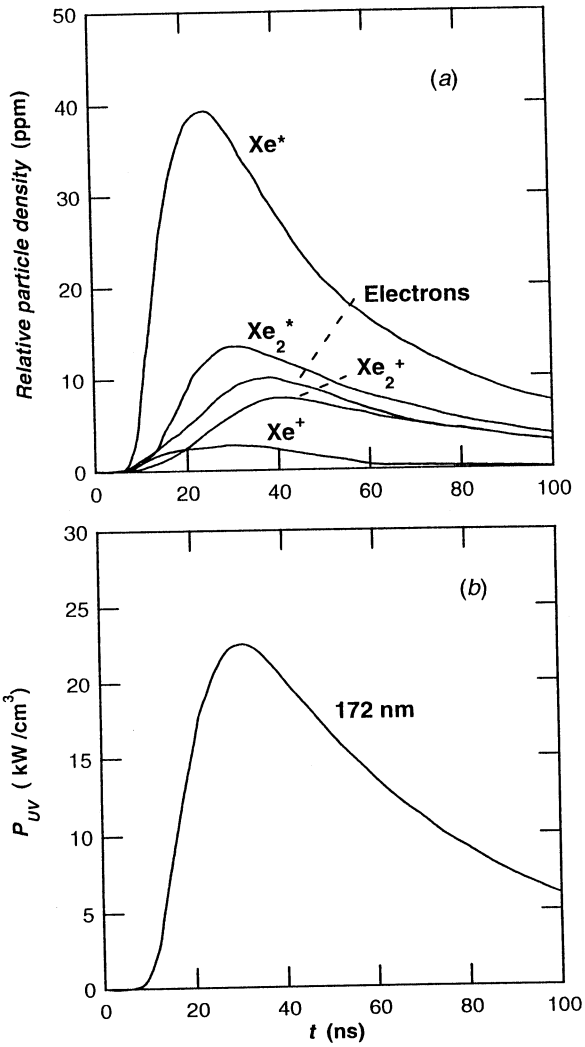

Fig. 3. (*a*) Calculated relative particle densities as a function of time in a microdischarge in xenon (from Eliasson and Kogelschatz 1991*b*). (*b*) Calculated 172 nm UV output from xenon excimers as a function of time in a dielectric barrier discharge (from Eliasson and Kogelschatz 1991*b*).

in the discharge column, the current declines and the microdischarge eventually extinguishes. Pietsch *et al.* proposed that any plasma chemical reactions would probably occur in the decay phase because the others are either too transitory or have an insufficient electron number density to have any effect.

5. The CQU–ANU Collaborative Venture

The experimental apparatus is currently under construction and consists of a dielectric barrier discharge source mounted on a linear motion feedthrough inside a bakeable UHV chamber with two magnesium fluoride viewports for

source observation. To maintain gas cleanliness, the chamber is evacuated by a turbomolecular pump which can be isolated by a gate valve when experiments are in progress. An excimer forming mixture of known composition is prepared by leaking gases into an external mixing chamber and monitoring their partial pressures with an accurate capacitance manometer. The gas mixture is then admitted to the evacuated chamber to a known pressure determined by a second capacitance manometer.

The source consists of a parallel array of a solid electrode and a fine mesh, both made from stainless steel, mounted outside Suprasil quartz dielectric barriers. The mesh electrode will allow the source to be viewed along the axial direction of the microdischarges as well as perpendicular to the electrode array as there is some evidence that the preferred direction of photon emission may be along the microdischarge axis, although no explanation for this has yet been proposed. A variable frequency high voltage is applied to the mesh electrode with the solid electrode tied to ground. Photons produced in the discharge are collected by a UV sensitive photomultiplier viewing the source through magnesium fluoride optics and suitable narrow bandwidth filters. Initial experiments will focus on the Hg–rare gas and rare gas–halogen excimers to test the apparatus by verifying the results of Kogelschatz and co-workers. The intensity of radiation will be monitored as a function of variables such as mixture composition (including the influence of buffer gases), total chamber pressure, electrode and dielectric barrier material and geometry, voltage pulse characteristics and viable source operational lifetime. These experiments are aimed at describing the operation of the source as a function of its macroscopic operating parameters. An indication of the importance of such characterisation lies with a recent investigation by Okazaki *et al.* (1993) using a dielectric barrier discharge source to generate atmospheric pressure glow discharges in air, argon, oxygen and nitrogen. They showed that the transition from an atmospheric pressure glow discharge to a filamentary discharge could be arrested depending on the choice of gas mixture composition, dielectric materials and electrode geometry.

To investigate any operational dependence on driving voltage, a high voltage power supply capable of generating pulses of (8 kV at 100% duty cycle or 0–16 kV at 50% duty cycle over a frequency range of 200 Hz–40 kHz has been designed and constructed. The supply had to meet the specification of a constant high voltage, variable frequency output, relatively independent of source load, allowing different geometries of barrier discharge sources to be investigated. It is based on a pulse generator feeding two Insulated Gate Bipolar Transistors driving two high voltage transformers. The transformers are wound on Siemens PM 74/59 ferrite Potcores and incorporate four secondary windings decoupled by high voltage diodes to reduce parasitic capacitive effects. The results of this work will be presented in a forthcoming publication (Kraus *et al.* 1995).

To fully understand the operation of a dielectric barrier discharge device, the physical and chemical processes occurring in an individual microdischarge have to be investigated in detail. Spectrally resolved, spatiotemporal measurements of the species existing in the current filament are needed to characterise a microdischarge and provide sufficient data to stringently test current models of the discharge process. Spatiotemporal optical emission spectroscopy studies have already been undertaken on high frequency glow discharges, providing information on electron

impact excitation rates and the existence of fast secondary electrons in argon (Tochikubo *et al.* 1990; Colgan *et al.* 1991; Makabe *et al.* 1992; Djurovic *et al.* 1993) and helium (Flohr and Piel 1993). They have also been used in studies of Townsend discharges following the development of the so-called 'photon flux' technique (Wedding *et al.* 1985). It is one of the primary goals of this venture to extend and develop these methods to the study of transient discharge phenomena.

The experimental work will be supported by a detailed numerical simulation program. These studies will allow the rapid exploration of potential experimental configurations to establish the relative impact of experimental variables on the population of the excited states responsible for the UV output. Initially the theoretical modelling will follow the work of Eliasson (Egli and Eliasson 1989; Eliasson and Kogelschatz 1991*b*) and Morrow (Morrow and Sato 1990). These approaches involve several approximations commonly employed in discharge physics, some of which have been recently studied in the context of Townsend discharges (Brennan *et al.* 1990; Blevin and Kelly 1991) but their validity for application to non-LTE discharges still needs to be examined in detail.

6. Concluding Remarks

Despite the work that has been performed on dielectric barrier discharges, many unanswered questions remain concerning the plasma physics and chemistry occurring in these devices, especially in the case of UV generation. Insufficient effort has been directed towards a critical investigation of the interplay between the microscopic and macroscopic parameters governing their operation. The key factor for optimising the performance of the sources for a wide range of physical conditions and processes will be an understanding of the detailed physics and chemistry occurring in the individual microdischarges. Our understanding of the development of the microdischarges both remote from, and near to, the dielectric boundaries needs to be improved. Specifically, we do not yet fully understand how the discharge propagates across the gap in an excimer gas mixture for example. The lifetime of a microdischarge is of the order of 10–100 ns and with a typical electrode separation of 1 cm, gas pressure of 1 atmosphere and electric field of 10 kV cm^{-1}, the drift velocity of the centre of mass of the electron swarm must be of the order of 10^6 m s^{-1} at $E/n \sim 40$ Td. Such speeds suggest that photoionisation ahead of the developing microdischarge may be important and this may have some connection with the observed preferred emission direction of the UV light from the barrier discharge. At the discharge/dielectric interface much is unknown. At typical pressures of the order of 1 atmosphere, the microdischarges appear uniformly distributed throughout the volume. It has been suggested that the presence of charge from a recent 'strike' on the dielectric precludes re-ignition of the discharge in the same channel on subsequent half cycles of the high voltage. However, there have been no definitive studies on how the charge dissipates itself along the dielectric after impact. It has also been suggested that there is negligible heating of the discharge channel but, once again, there is no supporting experimental evidence.

Spatial and temporal studies of the operation of the discharge will allow the distribution and evolution of the local densities of various species (excited neutrals and ions) and electron energy distribution functions to be determined. To be able to study these parameters simultaneously and with spectral resolution would yield

much useful information for improving the modeling of high pressure, transient discharges. It is the view of the authors that the development of techniques to undertake these types of experiments will be a major step forward towards fully understanding the operation of dielectric barrier discharges.

Acknowledgments

We wish to thank Drs J. Lowke and U. Kogelschatz for their helpful comments in fine tuning our research direction and Drs Gresser and Förster and Helmut Kraus for invaluable assistance in the design and construction of the discharge source power supply. We also acknowledge grants provided by CQU and ANU to undertake this work.

References

Bergonzo, P., and Boyd, I. W. (1993). *App. Phys. Lett.* **63**, 1757.
Bergonzo, P., Kogelschatz, U., and Boyd, I. W. (1993). *App. Surf. Sci.* **69**, 393.
Blevin, H. A., and Kelly, L. J. (1991). 'Gaseous Electronics and Its Applications' (Eds R. W. Crompton *et al.*), p. 127 (KTK Scientific: Tokyo).
Braun, D., Kuchler, U., and Pietsch, G. (1991). *J. Phys.* D **24**, 5642.
Brennan, M. J., Garvie, A. M., and Kelly, L. J. (1990). *Aust. J. Phys.* **43**, 27.
Colgan, M. J., Kwon, N., Li, Y., and Murnick, D. E. (1991). *Phys. Rev. Lett.* **66**, 1858.
Djurovic, S., Roberts, J. R., Sobelowski, M. A., and Olthoff, J. K. (1993). *J. Res. NIST* **98**, 159.
Eckstrom, D. J., Nakano, H. H., Lorents, D. C., Rothem, T., Betts, J. A., Lainhart, M. E., Dakin, D. A., and Maenchen, J. E. (1988). *J. Appl. Phys.* **64**, 1679.
Egli, W., and Eliasson, B. (1989). *Helv. Phys. Acta* **62**, 302.
Eliasson, B., and Egli, W. (1987). *Helv. Phys. Acta* **60**, 241.
Eliasson, B., and Gellert, B. (1990). *J. Appl. Phys.* **68**, 2026.
Eliasson, B., Hirth, M., and Kogelschatz, U. (1987). *J. Phys.* D **20**, 1421.
Eliasson, B., and Kogelschatz, U. (1988). *Appl. Phys.* B **46**, 299.
Eliasson, B., and Kogelschatz, U. (1991*a*). *Ozone Sci. & Eng.* **13** 365.
Eliasson, B., and Kogelschatz, U. (1991*b*). *IEEE Trans. Plasma Sci.* **19**, 309.
Esrom, H., and Kogelschatz, U. (1992). *Thin Solid Films* **218**, 231.
Flohr, R., and Piel, A. (1993). *Phys. Rev. Lett.* **70**, 1108.
Gellert, B., and Kogelschatz, U. (1991). *Appl. Phys.* B **52**, 14.
Gerber, T., Luethy, W., and Burkhard, P. (1980). *Opt. Commun.* **35**, 242.
Hopfield, J. J. (1930*a*). *Phys. Rev.* **35**, 1133.
Hopfield, J. J. (1930*b*). *Phys. Rev.* **36**, 784.
Hopfield, J. J. (1930*c*). *Astrophys. J.* **72**, 133.
Huffman, R. E., Tanaka, Y., and Larrabee, J. C. (1963). *Appl. Optics* **2**, 617.
Kogelschatz, U. (1993). 'Non-thermal Plasma Techniques for Pollution Control', NATO ASI Series, Vol. G34B (Eds B. J. Penetrante and S. M. Schultheis), p. 339 (Springer: Berlin).
Kraus, H., Gresser, H., Brennan, M. J., Newman, D. S., and Förster, H. (1995). *Meas. Sci. & Technol.* (in preparation).
Kumagai, H., and Obara, M. (1989*a*). *Appl. Phys. Lett.* **54**, 2619.
Kumagai, H., and Obara, M. (1989*b*). *Appl. Phys. Lett.* **55**, 1583.
Kumagai, H., and Obara, M. (1989*c*). *Japan. J. Appl. Phys.* **28**, L2228.
Lindau, D., and Dobele, H. F. (1988). *Rev. Sci. Instrum.* **59**, 565.
McLennan, J. C., and Turnbull, R. (1930). *Proc. R. Soc. London* **129**, 266.
McLennan, J. C., and Turnbull, R. (1933). *Proc. R. Soc. London* **133**, 683.
Makabe, T., Nakano, N., and Yamaguchi, Y. (1992). *Phys. Rev.* A **45**, 2520.
Manfredotti, C., Fizzotti, F., Osenga, C., Amato, G., and Boarino, L. (1993). *Phys. Status Solidi* A **135**, 191.
Morrow, R., and Sato, N. (1992). Proc. Tenth Int. Conf. on Gas Discharges and Applications, Swansea (Ed. W. T. Williams), p. 900.

Mukaida, M., Osato, K., Watanabe, A., Imai, Y., Kameyama, T., and Fukuda, K. (1993). *Thin Solid Films* **232**, 180.
Nakamura, I., Kannari, F., and Obara, M. (1990). *Appl. Phys. Lett.* **57**, 2057.
Nohr, R. S., MacDonald, J. G., Kogelschatz, U., Mark, G., Schuchmann, H.-P., and von Sonntag, C. (1994). *J. Photochem. Photobiol.* A **79**, 141.
Okazaki, S., Kogama, M., Uehara, M., and Kimura, Y. (1993). *J. Phys.* D **26**, 889.
Pavlovskaya, E. N., and Yakovleva, A. V. (1983). *Opt. Spectrosc. (USSR)* **54**, 132.
Pietsch, G. J., Braun, D., and Gibalov, V. I. (1993). 'Non-thermal Plasma Techniques for Pollution Control', NATO ASI Series, Vol. G34A (Eds B. J. Penetrante and S. M. Schultheis), p. 273 (Springer: Berlin).
Shevera, V. S., and Shuaibov, A. K. (1980). *Sov. Phys. Tech. Phys.* **25**, 434.
Shuaibov, A. K., and Shevera, V. S. (1979). *Sov. Phys. Tech. Phys.* **24**, 976.
Siemens, W. (1857). *Ann. Phys. Chem.* **106**, 66.
Tanaka, Y. (1955). *J. Opt. Soc. Am.* **45**, 710.
Tanaka, Y., and Zelikoff, M. (1954*a*). *J. Opt. Soc. Am.* **44**, 254.
Tanaka, Y., and Zelikoff, M. (1954*b*). *Phys. Rev.* **93**, 933.
Tochikubo, F., Kokubo, T., Kakuta, S., Suzuki, A., and Makabe, T. (1990). *J. Phys.* D **23**, 1184.
Volkova, G. A., Kirillova, N. N., Pavlovskaya, E. N., and Yakovleva, A. V. (1984). *J. Appl. Spectrosc. (USSR)* **41**, 1194.
Wedding, A. B., Blevin, H. A., and Fletcher, J. (1985). *J. Phys.* D **18**, 2361.
Wieme, W., and Lenaerts, J. (1981). *J. Chem. Phys.* **74**, 483.
Wilkinson, P. G., and Byram, E. T. (1965). *Appl. Opt.* **4**, 581.
Xiong, F. L., Wang, Y. Y., Leppert, V., and Chang, R. P. H. (1993). *J. Mater. Res.* **8**, 2265.
Yagi, S., Kuzomoto, M., and Nitta, T. (1989). *IEEE Denshi Tokyo* **28**, 39.
Zhang, J. Y., Esrom, H., Kogelschatz, U., and Emig, G. (1993). *Appl. Surf. Sci.* **69**, 299.
Zhang, J. Y., Esrom, H., Kogelschatz, U., and Emig, G. (1994). *J. Adhesion Sci. Technol.* **8**, 1179.

Manuscript received 10 October 1994, accepted 1 February 1995